Structure of Phospholipid Monolayers Containing Poly(ethylene glycol) Lipids at the Air−Water Interface

J. Majewski,[†,⊥] T. L. Kuhl,[‡] M. C. Gerstenberg,[§] J. N. Israelachvili,[‡] and G. S. Smith*[,†]

Manuel Lujan Neutron Scattering Center, Los Alamos National Laboratory, Los Alamos, New Mexico 87545, Department of Chemical Engineering, University of California, Santa Barbara, California 93106, and Department of Solid State Physics, Risø National Laboratory, DK-4000 Roskilde, Denmark

Received: August 23, 1996; In Final Form: February 6, 1997[⊗]

The density distribution of a lipid monolayer at the air−water interface mixed with varying amounts of lipid with poly(ethylene glycol) polymer headgroups (polymer−lipid or PEG−lipid) was measured using neutron reflectometry. The structure of the monolayer at the interface was greatly perturbed by the presence of the bulky polymer−lipid headgroups resulting in a large increase in the thickness of the headgroup region *normal* to the interface and a systematic roughening of the interface with increasing polymer−lipid content. These results show how bulky hydrophilic moieties cause significant deformations and out-of-plane protrusions of phospholipid monolayers and presumably bilayers, vesicles, and biological membranes. In terms of polymer physics, very short polymer chains tethered to the air−water interface follow scaling behavior with a mushroom to brush transition with increasing polymer grafting density.

Introduction

One of the more exciting ideas in the area of advanced drug delivery is the use of liposomes composed of macromolecular assemblies of lipids, cholesterol, and polymer-modified lipids (polymer−lipids) to encapsulate drugs.[1] By including a small percentage of polymer−lipids in the liposome membrane, the in vivo bloodstream half-life of the foreign liposomes is increased from hours to days due to the protection of the sterically stabilizing sheath of polymer chains extending from the liposome surface.[2−5] The polymer−lipid is generally a phosphatidyl ethanolamine of varying tail length with polyethylene glycol (PEG or EO_n of varying n) chemically grafted to the terminal amine of the headgroup.[6,7] Since PEG is a water-soluble polymer, when it is chemically bound to the lipid headgroup it acts as an enlarged hydrophilic headgroup for the molecule (Figure 1).

Previous work on the PEG−lipid system has focused on measuring the extension of the polymer chains from membrane surfaces through a variety of techniques: X-ray scattering of lamellae with different lipid/PEG−lipid compositions,[8] light scattering of PEG−lipid liposomes used for drug delivery,[9] force profiles of supported lipid bilayers matrixed with PEG−lipid using the surface forces apparatus,[10] electrophoresis of liposomes containing PEG covalently grafted to cholesterol molecules (which was used to determine the viscous drag of the polymer layer);[11] and finally, the disjoining pressure of a PEG−lipid monolayer interacting with a silicon oxide substrate was recently measured with ellipsometry.[12] Extensive monolayer studies have also been conducted detailing the phase behavior, surface potential, and lateral pressure as a function of area per molecule in lipid/PEG−lipid mixtures.[10,12−14]

Another method for probing the structure of polymers and lipids at interfaces is neutron reflectometry. In particular, polymers at the interfaces between solid surfaces and solvents have been the topic of several recent neutron reflectometry[15−18] and theoretical[19,20] studies. For grafted polymers in good solvent conditions, the density profile of the polymer as a function of surface coverage is a measure of the interaction between neighboring polymer chains. For instance, when the polymers are sparse on the surface, there will be little interaction between neighboring chains and the conformation will be that of a "mushroom".[16,19] On the other hand, as the polymer concentra-

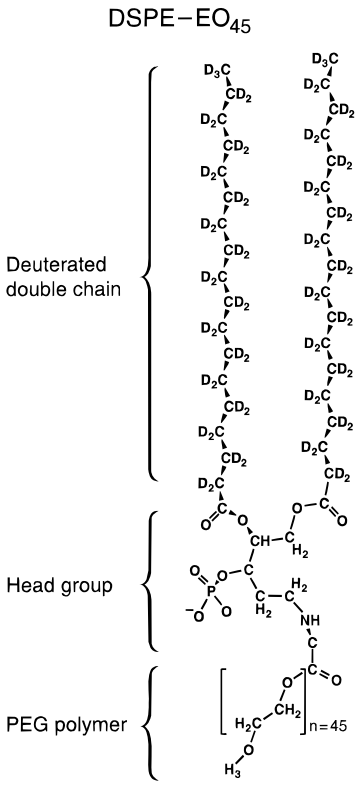

Figure 1. Model of the PEG−lipid molecule DSPE−EO_{45} showing the tail, headgroup, and polymer regions. In the experiments the tails were either hydrogenated (h) or deuterated (d). Case 1 was deuterated lipid tails on a D_2O subphase. Case 2 was hydrogenated lipids on a D_2O subphase. Case 3 was deuterated lipid tails on a mixed D_2O/H_2O subphase.

[†] Los Alamos National Laboratory.
[‡] University of California.
[§] Risø National Laboratory.
* To whom correspondence should be addressed.
[⊥] On leave from the Institute of Physics, Polish Academy of Sciences.
[⊗] Abstract published in *Advance ACS Abstracts,* April 1, 1997.

S1089-5647(96)02623-5 CCC: $14.00

tion increases, the polymers begin to overlap, interact, and extend away from the interface forming a "brush".[18,20] Such structures have been measured with adsorbed diblock copolymers (where one end of the diblock effectively "terminally grafts" the other block to a surface) using neutron reflectometry.[15−18] It is a straightforward extension to apply the same techniques to the study of biologically relevant PEG−lipids at the air−water interface, where the polymer surface coverage can be readily and quantitatively controlled between dilute mushrooms and concentrated brushes.[10,12,14,21]

To focus on the PEG−PEG interactions and how the structure of the phospholipid−solution interface is modified by the inclusion of bulky polymer−lipids, mixed monolayers of lipids matrixed with polymer−lipids were prepared on a Langmuir trough for study *via* neutron reflectometry experiments. The area per polymer chain was fixed by controlling the composition and surface pressure of the monolayer. The polymer chains can be thought of as tethered to the air−water interface. By varying the PEG−lipid concentration from 0 to 9% (mol of PEG−lipid/mol of total lipid), the polymer grafting density was varied from the mushroom through the brush regime.[8,10,21] To obtain further insight into how the polymer−polymer and polymer−lipid interactions affect the structure of phospholipid monolayers, the structure of such monolayers at the air−water interface was measured using neutron reflectivity.

Experimental Section

A. Materials. The spreading solutions were prepared by dissolving mixtures of disteroyl phosphatidyl ethanolamine DSPE (MW = 747) and the PEG−lipid DSPE−EO_{45} (MW = 2747) in 1:9 methanol:chloroform solution. The DSPE and DSPE−EO_{45} were purchased from Avanti Polar Lipids. They were >99% pure. The structure of the DSPE−EO_{45} molecule is shown in Figure 1. The PEG portion of the DSPE−EO_{45} had a molecular weight of 2000 (i.e., $n = 45$ monomers) and a polydispersity of <1.1. To enhance neutron scattering contrast, both hydrogenated (h) and deuterated (d) tails of the pure lipids and PEG−lipids were studied. The chloroform and methanol were of HPLC grade from Sigma. The mixtures were prepared by separately weighing and dissolving DSPE (1×10^{-3} M) and DSPE−EO_{45} (5×10^{-4} M) and mixing them in the correct proportions to yield the proper molar ratios. The four mixtures studied were 0.0, 1.3, 4.5, and 9.0 mol % of PEG−lipid. The subphase consisted of 99.8% isotopically pure D_2O (Sigma), H_2O (Millipore), or mixtures of both.

B. Langmuir Trough. The in situ Langmuir trough suitable for neutron reflectivity studies of monolayers on a liquid subphase was fashioned after a design previously used for X-ray scattering experiments.[22] The trough was constructed from a solid Teflon frame with internal dimensions of $160 \times 300 \times 16$ mm^3. This frame was bolted to an aluminum plate covered with a thin Teflon sheet, thereby forming the bottom of the trough. The aluminum plate had channels running through it such that thermostated water could be circulated to control the temperature. A solid Teflon barrier was placed across the trough and attached to a drive screw. The drive screw was turned by a stepping motor in order to position the barrier, thus varying the surface area of the trough. The trough was enclosed in a sealed aluminum canister so that evaporation of the subphase was minimized. Amorphous quartz windows, 2 mm thick, were mounted in the side walls of the canister to allow for passage of the neutron beam. A schematic of the trough and a monolayer are shown in Figure 2. The surface pressure was measured with a NIMA Model 9000 tensiometer using filter paper plates. Before experiments, the tensiometer was calibrated with arachidic acid. To reduce surface capillary waves, a very smooth glass block was placed in the trough just under the liquid subphase. This provided for a thin liquid film about 0.3 mm thick, beneath the footprint of the neutron beam. In addition, the entire trough was placed on a Newport Instruments EVIS active vibration isolation table to reduce external floor vibration.

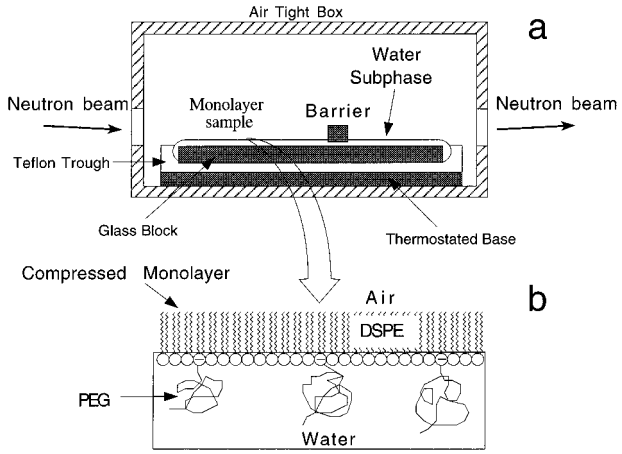

Figure 2. (a) Schematic view of the Langmuir trough used for the neutron scattering experiments. The glass block provides for a thin liquid film (about 0.3 mm thick) which effectively reduces surface capillary waves. (b) Blowup of a compressed lipid/PEG−lipid monolayer film at the air−water interface.

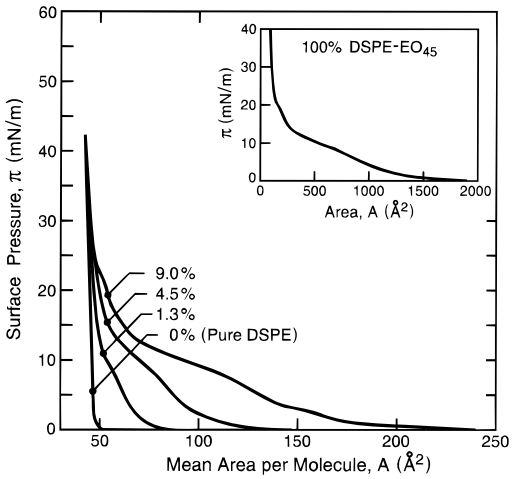

Figure 3. Monolayer compression ($\Pi-A$) isotherms of mixed DSPE/DSPE−EO_{45} at 21 °C. The area, A, is the mean area per molecule at the air−water interface. At high surface pressures (Π > 30 mN/m), the lateral interactions of the polymer chains are not evident in the surface pressure isotherms, as the polymer chains are completely submerged in the water subphase.[14,24] The inset is the isotherm for 100 mol % DSPE−EO_{45}.

Monolayers were prepared by spreading approximately 150 μL of lipid solution on the aqueous subphase, thus fixing the number of molecules on the surface. After waiting for the spreading solvent to evaporate, the pressure−area isotherm of the deposited lipid mixture was measured (Figure 3). For the neutron reflection experiments the surface pressure was kept at $\Pi = 40-45$ mN/m corresponding to a mean area per lipid molecule of about 43 Å^2. The temperature of the subphase was 21 ± 1.0 °C.

C. Neutron Reflectometer. The neutron measurements were made on the SPEAR reflectometer at the Manuel Lujan Jr. Neutron Scattering Center (MLNSC) at the Los Alamos National Laboratory. The range of neutron wavelengths was 1−16 Å. SPEAR's bulk shield collimation defines two separate beams, one at 0.9° and the other at 1.4°. The 0.9° beam was

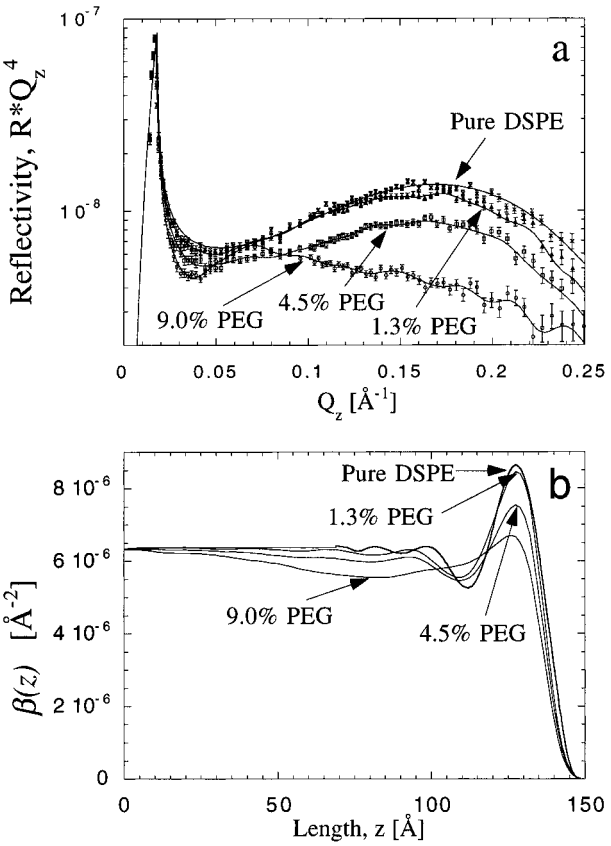

Figure 4. (a) Neutron reflectivity data for lipid/PEG−lipid monolayers on a pure D_2O subphase. The four reflectivity curves correspond to a pure DSPE monolayer and to mixtures of DSPE and DSPE−EO_{45}. In this set of data, all of the DSPE and DSPE−EO_{45} lipid hydrocarbon chains were fully deuterated (case 1). Full lines represent free form fits to the individual measurements. (b) Corresponding scattering length densities ($\beta(z)$) obtained from the fits shown in (a).

used to obtain the critical edge and the perpendicular scattering vector Q_z values from 0.01 to 0.1 Å^{-1} ($Q_z = 4\pi \sin \alpha/\lambda$, where α is the angle of incidence), while the 1.4° beam measures the Q_z range from 0.03 to 0.3 Å^{-1} and reflectivities with reasonable statistics to values of $R \sim 10^{-6}$. Typical counting times to study the monolayer samples were 1.5 and 8−9 h for the 0.9° and 1.4° beams, respectively. The reflected neutrons were counted using an Ordela Model 1202N linear position sensitive ^{3}He detector. The data were reduced and plotted as RQ_z^4 versus the perpendicular scattering vector, Q_z (this accounts for a sharp Q_z^{-4} decrease of the reflectivity due to the Fresnel's law, Figures 4 and 6−8). The error bars on the data represent the statistical errors in the measurements (standard deviation, σ_R) where the uncertainty in the Q_z resolution, σ_{Q_z}/Q_z, was nearly constant over this scattering vector range with a value of ~3%.[23]

Results

A. Pressure−Area Isotherms. We have previously reported on the lateral phase behavior of these lipid monolayers at the air−water interface and repeat only the salient details.[10,14] Figure 3 shows the surface pressure−area (Π−A) curves of unmodified DSPE doped with the various concentrations of DSPE−EO_{45} used in this study (0, 1.3, 4.5, 9.0 mol %) at 21 ± 1 °C. At high surface pressures, Π > 30 mN/m, the lateral interactions of the polymer chains are not evident in the surface pressure isotherm, as the polymer chains are completely submerged in the water subphase.[14,24] Thus, at high pressures none of the mixtures (1.3−9.0% DSPE−EO_{45}) are distinguishable from the pure DSPE case, and the surface pressure measurements are not sensitive to the lateral PEG−PEG interactions within the subphase.[14,24] To probe these interactions and to see if the physical structure of the monolayer was changing with increasing DSPE−EO_{45} content, the molecular density distributions of the mixed monolayers (0.0−9.0% DSPE−EO_{45}) at surface pressures of 40−45 mN/m were measured using neutron reflectometry.

B. Neutron Reflection Data. *(a) Free Form Fitting.* The neutron reflectivity data for deuterated monolayers on a pure D_2O subphase is shown in Figure 4a. The reflectivity measurements were initially analyzed using a one-step, free-form determination of the surface profiles.[25] In the free-form method, the scattering length density $\beta(z)$ is expanded in a series of cubic b-splines $B_j(z)$:

$$\beta(z) = \sum_{j=1}^{N} a_j B_j(z)$$

where a_j are the coefficients to be determined, and the minimum number of terms, N, obeys the relation

$$N = \frac{z_{max} Q_{max}}{\pi} - 2$$

Here Q_{max} is the largest occurring momentum transfer and z_{max} is the distance over which all the variation in $\beta(z)$ occurs. If z_{max} is chosen to be too small, oscillatory behavior of $\beta(z)$ at large z values occurs and the reflectivity data cannot be accurately fit. A typical scan has $Q_{max} = 0.25$ Å^{-1} and z_{max} as 300 Å, which gives a minimum value for N of approximately 22. N was actually set to 31 in order to further diminish short-period oscillations (ringing) in $\beta(z)$.

A nonlinear least-squares method (Marquardt−Levenberg) is used to minimize χ^2 given by

$$\chi^2 = \sum_{i=1}^{M} \frac{[R(Q_i)_{exp} - R(Q_i)]^2}{\sigma_i^2}$$

where $R(Q_i)$ is the reflectivity calculated dynamically from $\beta(z)$, $R(Q_i)_{exp}$ is the experimental data, and σ_i is the measured uncertainty of each data point. To overcome the problem of slow convergence and solutions with large oscillatory behavior, two constraints are included:

$$A_1 = \sum_{n=1}^{N-1} (a_{n+1} - a_n)^2 + w_1 a_1^2$$

$$A_2 = \sum_{n=1}^{N-1} (a_n - a_{av})^2 \qquad a_{av} = {}^1/_6 \beta_{av}$$

The first constraint measures the smoothness of the solution and the second biases the solution toward the expected average scattering length density. They can be transformed into a general constraint:

$$N_C = \left[(1 - w)A_1(N + 3) + w\frac{105A_2}{N + 3}\right]M$$

If $w = 0.5$, the two constraints contribute with equal weight, but $w = 0.1$ was used to assign a greater weight to the smoothness constraint, A_1. Introduction of the general constraint changes the function to be minimized to $\chi^2 + \lambda N_C$, where λ is a Lagrangian multiplier. The optimum value of the parameter λ is found from a discrepancy criterion using the mean-square

residual $MSR = \chi^2/M$. The constant λ is varied from 10^3 to 10^{-2} in equidistant steps on a logarithmic scale. For small values of λ, MSR is nearly constant, while MSR increases sharply for larger values of λ, in which case an overdamped solution to the reflectivity curve is obtained. The optimum value of λ is that which gives approximately a 10% increase in MSR relative to the lowest value of MSR.[25]

The free form fits to the reflectivity data on the pure D_2O subphase are shown as solid lines in Figure 4a. The corresponding scattering length density profiles are shown in Figure 4b. The air interface is at $z = 150$ Å. The large peak in the profile is due to the highly scattering deuterated lipid tails, while the following dip (which is barely visible for the 9% case) is the lipid headgroup. Finally, the long feature extending from the headgroup into the D_2O subphase is consistent with the attached PEG chains. From these free form profiles, several observations can be made. First, the lipid tail region $\beta(z)$ is decreasing in magnitude and width with higher DSPE−EO_{45} concentration. For $\beta(z)$ to decrease, the chain region must mix with some of the nearby regions of lower scattering length density, e.g., air, D_2O, or the lipid headgroup region.[24] This overall lower scattering length density combined with the narrowing of the lipid tail region suggests that this mixing is accomplished through a smearing or roughening of the entire air−water/lipid interface. This trend is also seen in the lipid headgroup region, where the dip in the $\beta(z)$ profile corresponding to the position of the lipid headgroups both decreases and broadens with increasing polymer−lipid concentration. Thus, with increasing polymer concentration the whole interface or monolayer structure is becoming increasingly rough in the z direction, i.e., out of the monolayer plane.

Another difference in the lipid region is seen with 9.0% DSPE−EO_{45}, where the dip in the scattering density due to the lipid headgroups is diminished at this high concentration. This can again be due to the smearing of the interface, or it could be suggestive of a change in the polymer structure at the polymer−headgroup boundary (i.e., there may be no depletion layer at this concentration). Polymer depletion at the interface region will be addressed fully later.

In terms of the polymer layer, after the dip from the lipid headgroup region the increase in polymer concentration with increasing DSPE−EO_{45} content is easily discernible in the free form fits as a decrease in the scattering length density from that of pure D_2O ($\beta_{D_2O} = 6.4 \times 10^{-6}$ Å^{-2}). Moreover, the ratio of this decrease and the distance over which it occurs qualitatively follows that expected for the three concentrations, 1.3, 4.5, and 9.0% DSPE−EO_{45}.

While free form analysis of the data yields some powerful general features of the scattering length density profiles, it is hard to obtain quantitative numbers for the thicknesses and scattering length densities of the individual components of the monolayer, e.g., headgroup, tail, and polymer layer. This problem is further compounded by the fact that this fitting procedure yields artifacts such as the oscillations shown in $\beta(z)$ in the vicinity of 50−100 Å, Figure 4b. To obtain more quantitative numbers and to better describe the monolayer structure, we used this analysis as a guide to developing a physically meaningful model which will be fit to the data in the next section.

(b) Model Fitting. Figure 5 shows the features of the simplest yet most physically reasonable models that fit the experimental data. Only case 1 where the lipid tails are deuterated is shown for simplicity. The starting point, Figure 5a, was that of a two-layer box model for the pure DSPE monolayer. For the PEG portion of the molecule, two different functional forms were used. The first, shown in Figure 5c, represents the case for a close-packed polymer brush. For the brush, the density profile of the polymer layer is parabolic[15,20] with a maximum at the headgroup interface. On the other hand, if the PEG is more like a polymer mushroom,[16,19,26] there is a depletion layer near the headgroup (i.e., a layer which has very little PEG and is mostly water) and a maximum polymer density some distance away from that interface. To model the depletion layer, one additional box was added between the headgroup box and the parabola representing the polymer layer (Figure 5b). (All the data were fit with and without the depletion layer.) The final feature of the model fits was the addition of smearing to the box models shown in Figure 5. To accomplish this, the box models were convoluted with a Gaussian smearing function to obtain the final form of the $\beta(z)$ profile:

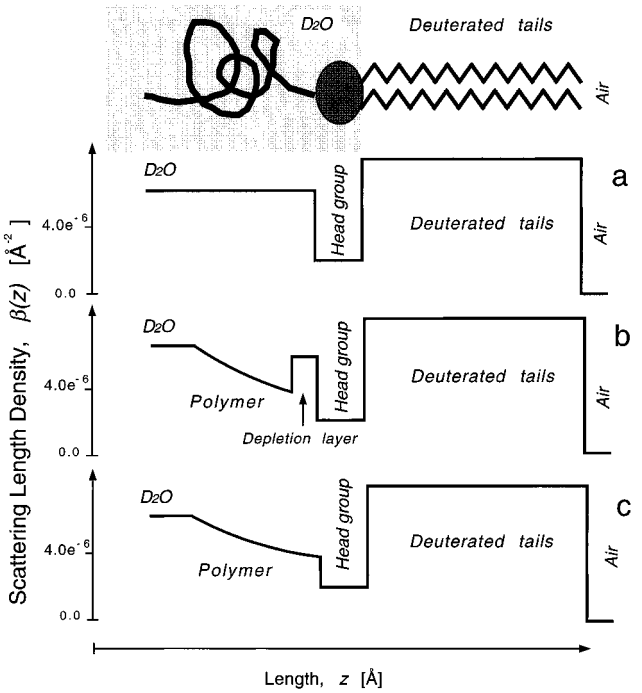

Figure 5. Schematic illustration of the PEG−lipid (deuterated tails, case 1) at the air/D_2O interface showing basic features of the model which has been chosen to fit the data. (a) The simplest case is a two-box model for the lipid tails and headgroup. For the PEG portion of the molecule, two different functional forms were used. (b) Polymer mushroom layer, where there is a depletion layer near the headgroup and a maximum polymer density occurring at some distance away from that interface. To accommodate the depletion layer, one additional box was added between the headgroup box and the parabola representing the polymer layer. (c) Case of a close-packed polymer brush: no depletion layer is assumed and the density profile of the polymer is parabolic with its maximum at the headgroup interface.

$$\beta(z) = \frac{1}{\sigma\sqrt{2\pi}}\int_{-\infty}^{\infty}\beta(z')e^{-(z-z')^2/2\sigma^2}\,dz'$$

where σ is the standard deviation of the Gaussian smearing function, and $\beta(z)$ is the scattering length density profile. To numerically approximate this $\beta(z)$ function, several small slabs (each ~1 Å thick) were used. The values of the reflectivity were calculated using this $\beta(z)$, and χ^2 was minimized with a Marquardt−Levenberg nonlinear least-squares fitting routine to obtain the best-fitting parameters.

The experimental data and the fits (solid lines) using the models described above are shown in Figures 6a, 7a, and 8a. Figures 6b, 7b, and 8b show the resulting $\beta(z)$ profiles. Figure 6 shows the data for a pure D_2O subphase and all deuterated

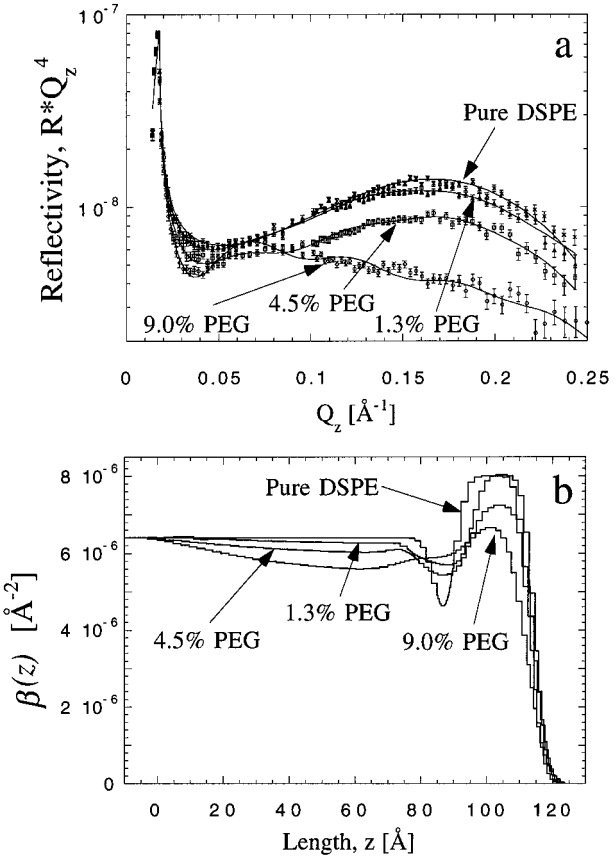

Figure 6. (a) Neutron reflectivity data for deuterated lipid/PEG−lipid monolayers on a pure D_2O subphase (case 1). The four reflectivity curves correspond to a pure DSPE monolayer and to mixtures of DSPE and DSPE−EO_{45}. Full lines represent fits to the individual measurements based on the models illustrated in Figure 5 and discussed in the text. Values for the fitted parameters are listed in Table 1. (b) Corresponding scattering length densities ($\beta(z)$) obtained from the fits.

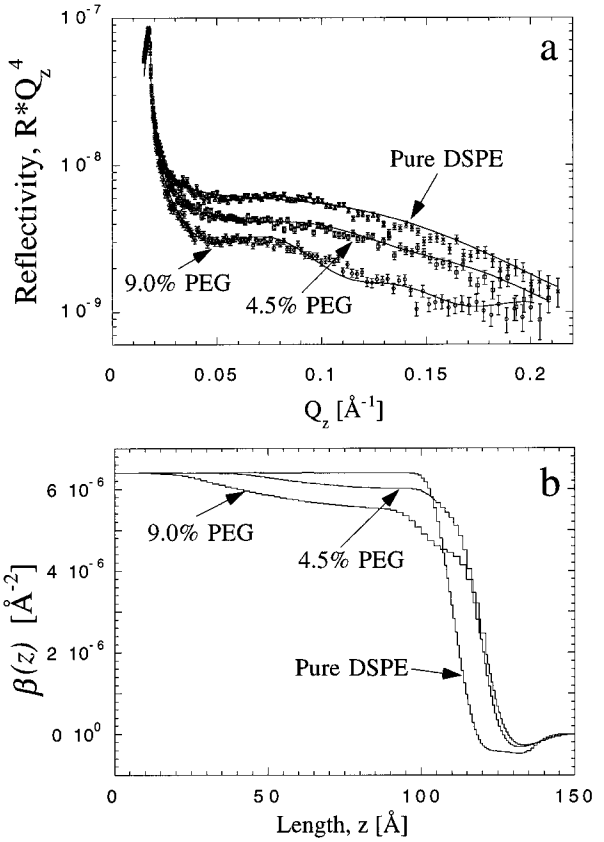

Figure 7. (a) Neutron reflectivity data for lipid/PEG−lipid monolayers on a pure D_2O subphase. The three reflectivity curves correspond to a pure DSPE monolayer and to 4.5 and 9.0% mixtures of DSPE and DSPE−EO_{45}. In this set of data, the DSPE and DSPE−EO_{45} lipid hydrocarbon chains were hydrogenated (case 2). Full lines represent fits to the individual measurements based on box models illustrated in Figure 5 and discussed in the text. Values for the fitted parameters are listed in Table 1. (b) Corresponding scattering length densities ($\beta(z)$) obtained from the fits.

lipid tails (case 1). In Figure 7, the data are for hydrogenated lipid tails and a pure D_2O subphase (case 2), and Figure 8 shows the results for deuterated tails and a D_2O/H_2O mixture which nearly contrast matches the headgroup/polymer region (case 3). In Table 1, the resulting fitting parameters are listed for each case. The $\beta(z)$'s and the thicknesses given in the table are for the unsmeared boxes which were convoluted using the value of σ given in column 1.

Discussion

A. Monolayer Structure. By examining the results in Figures 6−8 and Table 1, several observations can be made. First, the values obtained in this study for the pure DSPE monolayer are consistent with those previously measured on lipid samples with X-rays.[27] From the X-ray studies, reported values for the lipid head and tail lengths are 7.6 and 24.0 Å, respectively. Here, the average values were 5.9 and 22.1 Å. Using an average area per molecule of 43 $Å^2$, the calculated $\beta(z)$'s (in 10^{-6} units) are 2.5, −0.4, and 7.7 $Å^{-2}$, for the lipid heads, hydrogenated tails, and deuterated tails, respectively, while the average measured values were 3.0, −0.4, and 8.1 $Å^{-2}$. In addition, the surface roughness (i.e., the σ of the smearing function) has an average value of 3.3 Å. This value is also consistent with previous measurements of roughness due to capillary waves at the air−monolayer−water interface.[28,29]

In the analysis of the mixed DSPE/DSPE−EO_{45} monolayers, the initial focus will be on the structure of the lipid monolayer as a function of polymer−lipid concentration and then on the structure of the polymer layer itself. The fits to the data in Figures 6−8 for the mixed lipid system are summarized in Table 1. First, it can be seen that the surface roughness (or σ of smearing) increases with increasing DSPE−EO_{45} concentration. Second, the thickness of the total lipid layer (lipid tail + head box, column 2) increases with increasing polymer lipid content. The increased smearing of the interface accounts for some of the broadening of the features and also produces a decrease in the apparent lipid tail $\beta(z)$ as seen in Figures 6−8. However, in the fits, the $\beta(z)$'s and layer thicknesses were purposely permitted to vary to compensate for any inadequacies of a three-box model with only random Gaussian roughness (Figure 5). Examining the results for case 1 in detail, there is a general increase in both the $\beta(z)$ and thickness of the headgroup region and a decrease in the $\beta(z)$ and thickness of the tail region with increasing DSPE−EO_{45} content. Since the polymer chains cannot penetrate into the lipid tail region,[24] the decreasing $\beta(z)$ of the tails can be accomplished only by a mixing with air due to roughening of the lipid layer (Figure 9). Also, consistent with this effect, the $\beta(z)$ of the headgroup region and its thickness increase due to a complex mixing with the highly scattering deuterated lipid tails, D_2O subphase, and the less scattering PEG chains. The decrease in the thickness of the lipid tail region is more than compensated for by the increase in the thickness of the headgroup region, as clearly shown by the increase in the total lipid layer thickness with increasing polymer−lipid. Taken together, the results suggest that the interface is more complicated than uniform density boxes with

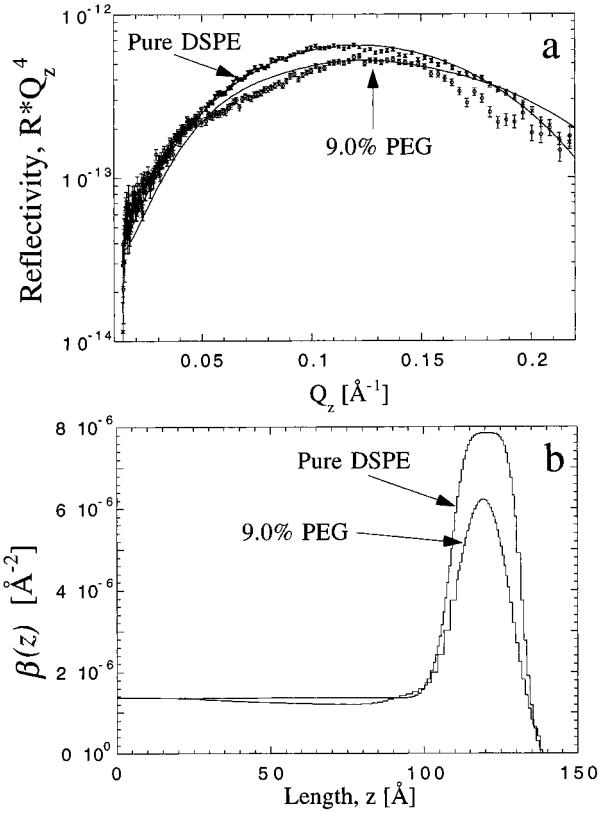

Figure 8. (a) Neutron reflectivity data for deuterated DSPE and 9.0% DSPE−EO_{45} on 0.3:0.7 (by weight) mixture of D_2O and H_2O subphase (case 3). Full lines represent fits to the individual measurements based on box models illustrated in Figure 5 and discussed in the text. Values for the fitted parameters are listed in Table 1. (b) Corresponding scattering length densities (β(z)) obtained from the fits.

Gaussian roughness. However, the freedom of the parameters to vary allows the simple box model to average over the complex effects and capture the essential features of the monolayer structure, as further evidenced by the fact that these same effects are also consistenly observed in cases 2 and 3.[30]

To obtain a better understanding of the results, a few simple ideas and calculations can be applied. As shown schematically in Figure 9, the polymer lipids should have two effects on the structure of the monolayer: (i) the greater solubility of DSPE−EO_{45} will result in a higher density of protrusions out of the monolayer plane, and (ii) at the higher DSPE−EO_{45} concentrations (4.5 and 9.0%) the lateral repulsive polymer−polymer interaction could possibly modify the rigidity and/or the packing structure of the lipid monolayer.

(a) Molecular Protrusions. In terms of quantifying roughness of the lipid−air−water interface due to molecular protrusions, covalently grafting PEG chains to DSPE lipids should greatly increase the solubility of these lipids. Indeed, the critical micelle concentration (cmc) of DSPE is approximately 1×10^{-12} M,[31] while the cmc of DSPE−EO_{45} is over 5 orders of magnitude higher, 6×10^{-6} M.[9] This increased solubility will result in a higher number of protrusions from the monolayer interface into the aqueous subphase. Using simple mean-field arguments, it has been shown that the density, ρ, of protrusions assuming an exponential decay with distance out of the monolayer plane, z, is given by[32−34]

$$\rho(z) = \rho(z{=}0)\mathrm{e}^{-V/kT}$$

where $z = 0$ is referenced to the air−water interface. The maximum distance, z_{max}, is given by the length of a DSPE lipid, 28 Å, and the potential energy, V, is calculated using

$$V = -kT\ln(\mathrm{cmc})$$

and assumed to have the form αz. Thus

$$V = \alpha z = \left(-\frac{kT}{z_{\max}}\ln(\mathrm{cmc})\right)z$$

The density of protruding DSPE−EO_{45} lipids at a distance z from the air−water interface is therefore given by

$$\rho_{\mathrm{DSPE-EO_{45}}}(z) = \rho_{\mathrm{DSPE-EO_{45}}}(z{=}0)\mathrm{e}^{-0.6\text{Å}^{-1}z}$$

while for non-polymer-modified DSPE lipids

$$\rho_{\mathrm{DSPE}}(z) = \rho_{\mathrm{DSPE}}(z{=}0)\mathrm{e}^{-1.1\text{Å}^{-1}z}$$

Hence, the DSPE−EO_{45} lipids will be protruding from the bilayer in higher numbers and for longer distances than nonmodified DSPE lipids, resulting in both a roughening of the monolayer interface and a broadening of the entire lipid region due to these protrusions (Figure 9b,c, Table 1, columns 1 and 2).

(b) PEG−PEG Interactions and Monolayer Roughening. The lateral interactions between polymer chains in the subphase will

TABLE 1: Parameters from Box Model Fits[a]

composition	σ [Å]	T-lipid = T-tail + T-head [Å]	β-tail [10^{-6} Å^{-2}]	T-tail [Å]	β-head [10^{-6} Å^{-2}]	T-head [Å]	β-depletion layer [10^{-6} Å^{-2}]	T-depletion layer [Å]	β-start-parabola [10^{-6} Å^{-2}]	T-parabola [Å]	χ^2
(d) pure lipid on D_2O (case 1)	2.9	26.7	8.2	22.3	3.1	4.4					3.8
(h) pure lipid on D_2O (case 2)	3.7	28.7	−0.4	21.9	3.0	6.8					5.0
(d) pure lipid on 0.3 D_2O (case 3)	3.3	28.4	8.0	22.0	2.8	6.4					2.5
(d) 1.3% PEG on D_2O (case 1)	3.3	30.5	7.9	20.5	5.2	10.0	6.1	5.9	6.3	45.0	10.0
(d) 4.5% PEG on D_2O (case 1)	3.4	33.7	7.3	19.2	5.4	14.5	6.3	4.9	6.1	65.0	6.7
(h) 4.5% PEG on D_2O (case 2)	4.8	34.0	−0.4	19.5	5.3	14.5	6.2	4.8	6.0	60.0	5.7
(d) 9.0% PEG on D_2O (case 1)	4.5	39.5	6.8	18.5	5.9	21.0			5.6	75.0	7.1
(h) 9.0% PEG on D_2O (case 2)	4.9	39.0	−0.3	18.0	4.5	21.0			5.5	80.0	5.0
(d) 9.0% PEG on 0.3 D_2O (case 3)	5.5	38.8	6.8	18.2	1.5	20.6			1.2	70.0	8.2

[a] The parameters correspond to the box models shown in Figure 5. T refers to the thickness of the specified box in angstroms, and β to the scattering length density in Å^{-2}. σ is the fitted Gaussian roughness of the interface.

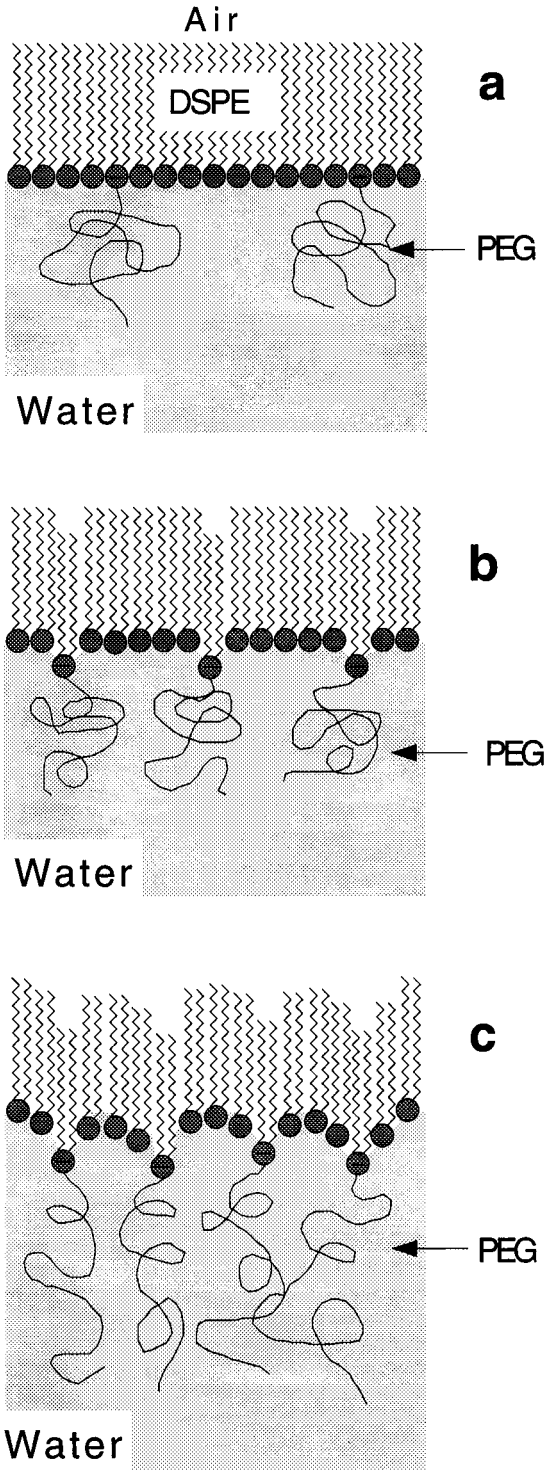

Figure 9. Schematic of the monolayer structure at the air−water interface. The increase in out-of-plane fluctuations greatly alters the monolayer structure, where (a) is a completely in-plane monolayer for reference at a concentrations of 1.3% DSPE−EO_{45}, (b) represents single molecular protrusions, and (c) represents roughening of the entire monolayer surface at the higher concentration of 9.0% DSPE−EO_{45}.

also affect the structure of the monolayer at the interface. In the case of grafted polymer chains to a stationary (rigid) surface, the balance between the osmotic pressure within the polymer layer and the elastic restoring force of the chains determines the polymer layer thickness. In a flexible monolayer system, some of the highly unfavorable osmotic pressure within the submerged polymer layer can be deceased by roughening the interface as depicted in Figure 9c. Although the average 2-D area per lipid molecule was held constant at about 43 $Å^2$ for all the DSPE−EO_{45} concentrations, staggering the lipids at the air−water interface increases the total surface area and thus *effectively* increases the area per lipid molecule. This increase in area, although interfacial energy costly, decreases the osmotic pressure within the polymer layer, since the osmotic pressure scales inversely with the area per polymer chain. Thus, qualitatively, the monolayer structure will also be modified by submerged PEG−PEG interactions.

In summary, the correlation between the changes in the $\beta(z)$'s and increase in thickness of the headgroup region and decrease in the thickness of the tail region with increasing DSPE−EO_{45} content implies that the bulky polymer is pulling the polymer−lipid further into the water subphase and broadening the entire lipid region (Table 1). While complicated protrusions and roughening are not fully captured by a simple Gaussian roughness, our models nevertheless show that these trends occur in each of the experimental cases (1−3).

B. Polymer Layer Density Distribution. In terms of modeling the density distribution of the PEG segments away from the monolayer, one of the most obvious differences in the mixed lipid system is the increase in the thickness of the parabola representing the polymer with increasing DSPE−EO_{45} concentration (Table 1). Moreover, this increase in the thickness of the polymer layer is greater than the additional extension due to smearing and as such is less sensitive to the smearing of the monolayer. Also, from Figures 6−8 the depth of the parabola increases with the increasing concentration. This is consistent, since a lower scattering length density is expected as more polymer ($\beta = 0.25 \times 10^{-6}$ $Å^{-2}$) displaces D_2O ($\beta = 6.4 \times 10^{-6}$ $Å^{-2}$, or D_2O/H_2O mix in case 3) with higher concentrations of DSPE−EO_{45}. Moreover, the thickness of the polymer layer (parabola) increases as expected with increasing DSPE−EO_{45} content as determined using other techniques.[8,10,11]

Since the Flory radius ($R_F = aN^{3/5}$, where a is the size of a monomer) of the PEG polymer is 35 Å,[10] it would be expected that once the area per molecule drops below $R_F^2 \approx 1000$ $Å^2$ that neighboring polymer chains begin to impinge on one another. From the $\Pi-A$ isotherms, the packing area per PEG chain is 3300, 960, and 480 $Å^2$ for the 1.3, 4.5, and 9.0 mol % DSPE−EO_{45}, respectively.[10] In this case, one would expect the 1.3% to be noninteracting mushrooms, 4.5% weakly interacting mushrooms, and 9.0% in the polymer brush regime.

Turning our attention to the fitted parameters for the polymer depletion layer (Table 1), for the lower DSPE−EO_{45} concentrations (1.3 and 4.5%) a polymer-depleted layer (Figure 5b) is required to fit the reflectometry profiles (Figures 6 and 7). In contrast, the 9% DSPE−EO_{45} data were well fit without a depletion layer. As with the free form fit, this again suggests that there is no depletion layer at this concentration. This behavior is similar to that seen in earlier neutron reflectivity studies of adsorbed monolayers of polystyrene(PS)−poly(ethylene oxide) (PEO) diblock copolymers.[16] In that study, it was found that a mushroom-to-brush transition in an adsorbed polymer monolayer could be induced by elevating the surface coverage of the PS blocks. The signature of this transition was that the density profile changes from one with a depletion layer near the solid/liquid interface (the Alexander−de Gennes model[19]) to a $\beta(z)$ with a parabolic density profile (the Milner, Cates, and Witten model[20]). Similarly, in the present study, the lower 1.3 and 4.5% mushroom regimes required a depletion layer, while the 9.0% concentration data could not be well fit with a depletion layer. However, the presence of the extended headgroup region at 9.0% prevents us from unambiguously determining whether a maximum in the polymer density occurs at the lipid surface.

Conclusions

Data from neutron reflectivity studies of lipid/PEG−lipid monolayers at the air−water interface have been presented. The PEG portions of the molecules extended into the water subphase, while the lipids were constrained to the interface. As the concentration of PEG−lipids in the monolayer increased, the extension of the PEG chains from the interface increased. Although a mushroom-to-brush transition in the polymer density distribution cannot be unambiguously reported, the data were consistent with this picture, as previously put forth for polymer diblocks. Significantly, the air−water interface proportionally roughens with the addition of PEG lipids. This roughening was attributed to two mechanisms: (a) an increase in lipid protrusions due to the increased solubility of the PEG−lipids; (b) to a relaxation of the lateral force between the PEG portions by staggering the lipids. Finally, these results also demonstrate that PEG−lipids provide an extended 40−75 Å (depending on the PEG−lipid concentration) thick polymer shield around biological membranes, which are currently being used as novel drug-delivery vehicles.

Acknowledgment. We would like to thank Kristian Kjaer and Jens Als-Nielsen for providing us with drawings of the Langmuir trough and sample canister used previously on the D4 beam line at HASYLAB, Steve Burgess and Avanti Polar Lipids for synthesizing the dueterated DSPE−EO_{45}, Jan Skov Pedersen for allowing us to use his FORTRAN code for free form reflectivity fitting, and Ross Sanchez for technical assistance in all modifications on the trough and sample canister. This work was partially supported by the U.S. Department of Energy under contract W-7405-ENG-36, the Department of Energy (DOE) under Grant DE-FG03-87ER45331, and benefited from the use of the SPEAR reflectometer at the Manuel Lujan Neutron Scattering Center, Los Alamos National Laboratory.

References and Notes

(1) Lasic, D.; Martin, F. *Stealth Liposomes*; CRC Press: Boca Raton, FL, 1995 and references therein.

(2) Klibanov, A. L.; Maruyama, K.; Torchillin, V. P.; Huang, L. *FEBS Lett*. **1990**, *268*, 235.

(3) Blume, G.; Cevc, G. *Biochim. Biophys. Acta* **1990**, *1029*, 91.

(4) Allen, T. M.; Hansen, C.; Martin, F.; Redemann, C.; Yau-Young, A. *Biochim. Biophys. Acta* **1991**, *1066*, 29.

(5) Papahadjopoulos, D.; Allen, T. M.; Gabizon, A.; Mayhew, E.; Matthay, K.; Huang, S. K.; Lee, K.-D.; Woodle, M. C.; Lasic, D. D.; Redemann, C.; Martin, F. J. *Proc. Natl. Acad. Sci. U.S.A.* **1991**, *88*, 11460.

(6) Zalipsky, S. *Adv. Drug Delivery Revs.* **1995**, *16*, 157.

(7) Woodle, D. R.; Lasic, D. D. *Biochim. Biophys. Acta.* **1992**, *1113*, 171 and references therein.

(8) Kenworthy A. K.; Hristova, K.; Needham, D.; McIntosh, T. J. *Biophys. J.* **1995**, *68*, 1921.

(9) Uster, P. S.; Allen, T. M.; Daniel, B. E.; Mendez, C. J.; Newman, M. S.; Zhu, G. Z. *FEBS Lett.* **1996**, *386*, 243.

(10) Kuhl, T.; Leckband, D.; Lasic, D.; Israelachvili, J. *Biophys. J*. **1994**, *66*, 1479.

(11) Janzen, J.; Song, X.; Brooks; D. E. *Biophys. J.* **1996**, *70*, 313.

(12) Baekmark, T. R.; Elender, G.; Lasic, D. D.; Sackmann, E. *Langmuir* **1995**, *11*, 3975.

(13) Rosilio, V.; Albrecht, G.; Okumura, Y.; Sunamoto, J.; Baszkin, A. *Biophys. J.* **1996**, *12*, 2544.

(14) Kuhl, T. L.; Leckband, D. E.; Lasic, D. D.; Israelachvili, J. N. *Modulation and modeling of interaction forces between lipid bilayer exposing terminally grafted polymer chains*. In *Stealth Liposomes*; Lasic, D., Martin, F., Eds.; CRC Press: Boca Raton, FL, 1995; pp 73−91.

(15) Field, J. B.; Toprakcioglu, C.; Ball, R. C.; Stanley, H.; Dai, L.; Barford, W.; Penfold, J.; Smith, G. S.; Hamilton, W. A. *Macromolecules* **1992**, *25*, 434.

(16) Field J. B.; Toprakcioglu, C.; Dai, L.; Hadziioannou, G.; Smith G. S.; Hamilton, W. A. *J. Phys. II* **1992**, *2*, 2221.

(17) Perahia, D.; Wiesler, D. G.; Satija, S. K.; Fetters, L. J.; Sinha, S. K.; Milner, S. T. *Phys. Rev. Lett.* **1994**, *72*, 100.

(18) Karim, A.; Satija, S. K.; Douglas, J. F.; Fetters, L. J. *Phys. Rev. Lett.* **1994**, *73*, 3407.

(19) Alexander, S. *J. Phys*. **1977**, *38*, 983. de Gennes, P. G. *Macromolecules* **1980**, *13*, 1069. de Gennes, P. G. *J. Phys.* **1976**, *37*, 1445.

(20) Milner, S.; Witten, T.; Cates, M. *Macromolecules* **1988**, *21*, 2610.

(21) It has been theoretically shown that very short PEG polymers (less than 20 monomers) should be reasonable models of random coils. Puvvada S.; Blankschtein, D. *J. Phys. Chem.* **1992**, *96*, 5579.

(22) Helm, C. A.; Möhwald, H.; Kjaer, K.; Als-Nielsen, J. *Biophys. J.* **1987**, *52*, 381.

(23) Smith, G. S.; Pynn, R.; Baker, S.; Fitzsimmons, M.; Xuan, L. *Los Alamos Neutron Scattering Center News Letter*, **1993**, no. 15, Spring.

(24) Low MW PEG has been shown to be excluded from the surface of phospholipid bilayers; i.e., the PEG chain does not penetrate into the lipid tail region nor does it adsorb to or interact with the lipid headgroups. Kuhl, T.; Guo, Y.; Alderfer, J. L.; Berman, A. D.; Leckband, D.; Israelachvili, J.; Hui, S. W. *Langmuir* **1996**, *12*, 3003. Arnold, K.; Pratsch, L.; Gawrisch, I. *Biochim. Biophys. Acta* **1983**, *728*, 121. Arnold, K.; Hermann, A.; Gawrisch, I.; Pratsch, L. *Stud. Biophys.* **1985**, *110*, 135. Arnold, K.; Lvov, Y. M.; Szogyi, M.; Gyorgyi, S. *Stud. Biophys*. **1986**, *113*, 7. Arnold, K.; Zschoernig, O.; Barthel, D.; Herold, W. *Biochim. Biophys. Acta* **1990**, *1022*, 303.

(25) Pedersen, J. S.; Hamley, I. W. *J. Appl. Crystallogr*. **1994**, *27*, 36.

(26) Kent, M. S.; Lee, L. T.; Factor, B. J.; Rondalez, F.; Smith, G. S. *J. Chem. Phys*. **1995**, *103*, 2320.

(27) Kjaer, K.; Als-Nielsen, J.; Helm, C. A.; Laxhuber, L. A.; Möhwald, H. *Phys. Rev. Lett*. **1987**, *58*, 2224. Helm, C. A.; Möhwald, H.; Kjaer, K.; Als-Nielsen, J. *Europhys. Lett.* **1987**, *4*, 697. Helm, C. A.; Tippman-Krayer, P.; Möhwald, H.; Als-Nielsen, J.; Kjaer, K. *Biophys. J.* **1991**, *60*, 1457.

(28) Braslau, A.; Deutsch, M.; Pershan, P. S.; Weiss, A. H.; Als-Nielsen, J.; Bohr, J. *Phys. Rev. Lett.* **1985**, *54*, 114.

(29) Braslau, A.; Pershan, P. S.; Swislow, G.; Ocko, B. M.; Als-Nielsen, J. *Phys. Rev. A* **1988**, *38*, 2457.

(30) More complicated models were also investigated. A multiple-box model with two tail boxes and two headgroup boxes did fit the reflectivity data quite well. In fact, the tail region could be fit with 1 box of lower scattering length density (tails + air) and a second inner box of constant scattering length density expected for close-packed hydrocarbon chains. However, the complexity of these models and the addition of more fitting parameters was difficult to justify with the resolution of the reflectivity data. Moreover, the salient details of the fits to the data were well captured by the simplier models used and described in Figure 5.

(31) Marsh, D. *Handbook of Lipid Bilayers*; CRC Press: Boca Raton, FL, 1990; p 387.

(32) Israelachvili, J. N.; Wennerstrom, H. *J. Phys. Chem*. **1992**, *96*, 520.

(33) Gordeliy, V. I. *Langmuir* **1996**, *12*, 3498−3502.

(34) Lipowsky, R.; Grotehans, S. *Biophys. Chem.* **1994**, *49*, 27−37.